OPEN ACCESS
JOURNAL OF ADVANCED DIELECTRICS
Vol. 13, No. 1 (2023) 2242004 (8 pages)

DOI: 10.1142/S2010135X22420048

High energy storage properties in $Ca_{0.7}La_{0.2}TiO_3$-modified $NaNbO_3$-based lead-free antiferroelectric ceramics

Cen Liang*,¶, Changyuan Wang*,¶, Wenjun Cao*, Hanyu Zhao*, Feng Li†,‡ and Chunchang Wang*,§

*Laboratory of Dielectric Functional Materials, School of Materials Science and Engineering Anhui University Hefei, Anhui 230601, P. R. China

†Information Materials and Intelligent Sensing Laboratory of Anhui Province Key Laboratory of Structure and Functional Regulation of Hybrid Materials of Ministry of Education, Institutes of Physical Science and Information Technology, Anhui University Hefei, Anhui 230601, P. R. China

‡fengli@ahu.edu.cn

§ccwang@ahu.edu.cn

Received 26 August 2022; Revised 16 September 2022; Accepted 25 September 2022; Published 17 November 2022

In this work, $(1-x)(0.92NaNbO_3-0.08BaTiO_3)-xCa_{0.7}La_{0.2}TiO_3$ (NNBT – xCLT) ceramics were successfully designed and prepared by the solid-state reaction method. Investigations on the structure, dielectric, and energy storage properties were performed. The NNBT – 0.25CLT ceramic with orthorhombic phase at room temperature was found to exhibit extremely small grain size and compacted microstructure. A large W_{rec} of 3.1 J/cm^3 and a high η of 91.5% under the electric field of 360 kV/cm were achieved simultaneously in the sample. In addition, the energy storage performance of the sample exhibits thermal stability over the temperature range of 25–140°C and the frequency range of 5–500 Hz. The charge and discharge tests reveal that the ceramic shows a large current density C_D of 965 A/cm^2 and power density P_D of 154 MW/cm^3. This work demonstrates that the NNBT–0.25CLT ceramic is a prospective energy storage material for potential application in the field of pulsed power devices.

Keywords: Lead-free $NaNbO_3$-based ceramics; phase transition; energy storage; charge discharge performance.

1. Introduction

Energy and environmental problems are the biggest challenges the world is facing today. How to reduce energy consumption, improve storage efficiency, and develop environmentally friendly renewable energy have become the focus of people's attention.[1–5] Among the majority of electrical energy storage devices, dielectric capacitors have many advantages, such as wide application temperature range, faster charge/discharge, high power density, and long service life.[3,4] The high-energy-storage-density dielectric capacitors can serve as power electronics used in electric vehicles. But the main problem of dielectric capacitor is the relatively low energy storage density (<30 Wh/kg).[4,6,7] If the energy storage density of the dielectric capacitor in pulsed power equipment can reach the level of electrochemical supercapacitors, it would make an important contribution in promoting miniaturization, weight reduction, and integration of components.[8,9] The total energy storage density (W_{total}), recoverable energy storage density (W_{rec}), and efficiency (η) of a dielectric capacitor can be calculated by the following mathematical formulae:

$$W_{total} = \int_0^{P_{max}} EdP, \tag{1}$$

$$W_{rec} = \int_{P_r}^{P_{max}} EdP, \tag{2}$$

$$\eta = \frac{W_{rec}}{W_{total}} \times 100\%, \tag{3}$$

where P_r and P_{max} are the remnant polarization and the maximum polarization under the applied electric field (E), respectively.[10,11]

Lead-free perovskite ceramics are one of the main energy storage materials. Among them, ferroelectrics (FEs), such as $Na_{0.5}Bi_{0.5}TiO_3$ (BNT), $BaTiO_3$ (BT), etc., have the characteristics of relatively high breakdown field (E_b) and optimal polarization.[12,13] Therefore, extensive research has been carried out on FE-based energy storage materials.[14–16] In recent years, investigations on antiferroelectric (AFE) ceramic materials have become more and more abundant,[17–21] because the electric field can induce AFE–FE phase transition leading to unique double polarization versus electric field (P–E) hysteresis loop and increased polarization difference ($\Delta P = P_{max} - P_r$).[22,23] However, the AFE ceramics usually show relatively low η owing to their large polarization hysteresis caused by the AFE–FE phase transition.[24] The introduction of secondary

¶These authors contributed equally to this work.

dielectric compounds into the AFE ceramics can depress the long-range AFE order, yielding relaxor AFE characterized by polar nanoregions (PNRs).[25] Finer *P–E* loops can be obtained in the relaxor AFE ceramics, which plays a positive influence in improving the energy storage characteristics.[26–29]

$NaNbO_3$ (NN) lead-free ceramics have AFE orthorhombic P-phase structure at room temperature, which converts to AFE orthorhombic R-phase with *Pnma* space group at high temperature.[22,30] By compositing perovskite with low tolerance factor (τ) or low polarizability, not only the stabilization of the AFE P-phase can be enhanced, but also the stabilized AFE R-phase can be obtained, giving rise to strong dielectric relaxation behavior and nanodomain morphology,[24,31] which, in turn, lead to a low polarization hysteresis and a large driving electric field of the phase transition (E_{AFE}), thereby improving the energy storage performance.[32]

Considering that the BT has stable phase structure and high resistivity, when the content of BT doped into NN ceramics is within 0.08–0.10, the orthorhombic and tetragonal phases coexist.[33,34] At the same time, $CaTiO_3$ (CT) has a large bandgap (E_g ~ 3.4 eV),[35,36] and La^{3+} ion is a common dopant for lead-free piezoelectric ceramics. So, the introduction of $Ca_{0.7}La_{0.2}TiO_3$ (CLT) into NN will tend to increase the value of E_b. On the atomic scale, the addition of CLT into NN will enhance the disorder of the composition. Limited by the radius of ions, Ca^{2+} (r = 1.34 Å) and La^{3+} (r = 1.36 Å) will preferentially replace the *A*-site Na^+ (r = 1.39 Å) and Ba^{2+} (r = 1.61 Å) ions. Whereas, Ti^{4+} (r = 0.61 Å) will replace Nb^{5+} (r = 0.64 Å) at the *B*-site. Both factors destroy the long-range FE order of ceramics and induce small-size PNRs. With small PNRs, they can quickly respond to electric field, thus greatly increasing the energy storage efficiency of the NN-based ceramics. Furthermore, CLT has a relatively low τ value. When it was added into the NN-based ceramics, the AFE R-phase was expected to be stabilized and the phase transition temperature of AFE P–R could be reduced.[24,37,38]

Therefore, $(1-x)(0.92NaNbO_3–0.08BaTiO_3)–xCa_{0.7}La_{0.2}TiO_3$ (NNBT–*x*CLT) ceramics were designed and prepared by the conventional solid-state reaction method in this work and their energy storage properties were investigated. Our results reveal that the NNBT–0.25CLT ceramic with pure AFE R-phase structure exhibits extremely small grain size and compacted microstructure. A large W_{rec} of 3.1 J/cm^3 and a high η of 91.5% were achieved simultaneously in the sample.

2. Experimental

Details of the experimental procedure and characterization of NNBT–*x*CLT ceramics are provided in Supplementary Material.

3. Results and Discussion

Figure 1 shows the XRD patterns of the NNBT–*x*CLT samples. It can be seen that all the samples exhibit a main perovskite structure, indicating that the CLT component has dissolved into the NN lattice. A careful examination reveals that there are three small peaks around 35–42° as indicated by three arrows at the pattern for the sample of x = 0.05, which are the typical AFE characteristic peaks.[18,31,39] In addition, from the enlarged view of the (110) and (200) peaks, peak splitting for both peaks is observed for the samples with $x \leq$ 0.10. This indicates that the AFE P-phase and AFE R-phase coexist in these ceramics as have been reported in recent articles.[24,31] For x = 0.10 ceramic, the peak split becomes inconspicuous indicating that the coexistence of the AFE P-phase and AFE R-phase gradually disappears. For the samples with $x \geq$ 0.15, only the AFE R-phase can be seen. Meanwhile,

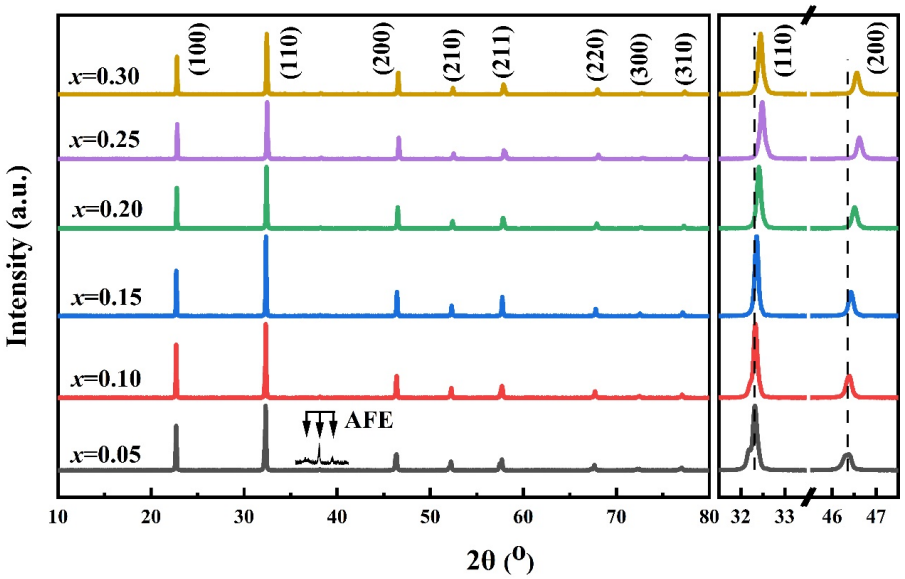

Fig. 1. XRD patterns of the NNBT–*x*CLT samples and an enlarged view of peaks in the ranges of 31.5–33.5° and 45.5–47.5°.

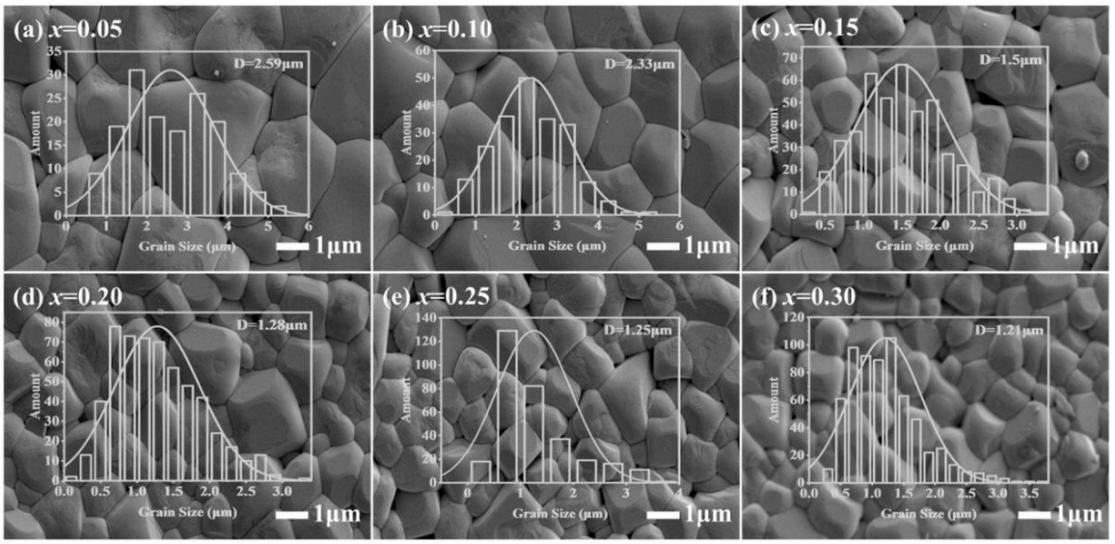

Fig. 2. SEM images and grain size distributions of the NNBT–*x*CLT ceramics.

both (110) and (200) peaks shift to higher angles as the CLT content increases. This fact indicates that CLT addition leads to the crystal lattice shrinkage, due to the fact that both the *A*-site dopants Ca^{2+} ($r = 1.34$ Å) and La^{3+} ($r = 1.36$ Å) and the *B*-site dopant Ti^{4+} ($r = 0.61$ Å) are smaller than the substituted ions as aforementioned.[32]

Figure 2 shows the SEM images of the NNBT–*x*CLT ceramics. A compacted microstructure without obvious pores is found for all the NNBT–*x*CLT ceramics. The grain size distribution was analyzed using Nano Measurer software and the statistical results were presented as insets in the corresponding figure of each sample. It is clearly seen that, as the CLT content increases from 0.05 to 0.30, the average grain size gradually decreases from 2.59 μm to 1.21 μm. This finding suggests that the CLT addition can inhibit the grain growth. A smaller grain size means the larger portion of grain boundary density. It shows that the total resistivity of the NNBT–*x*CLT ceramics is enhanced, because the grain boundary can better hinder the charge diffusion than grain. Denser microstructure helps to prevent a large amount of energy loss, thus improving the breakdown strength of ceramics.[27,40–42]

The variations of dielectric constant (ε_r) and loss tangent (tanδ) for the NNBT–*x*CLT ceramics with temperature over the frequency range of 100 Hz–1 MHz are shown in Fig. 3. It can be seen that when the CLT amount is 0.05, there is a dielectric abnormal peak representing the AFE P-phase–AFE R-phase transition with the transition temperature (T_{P-R}) near

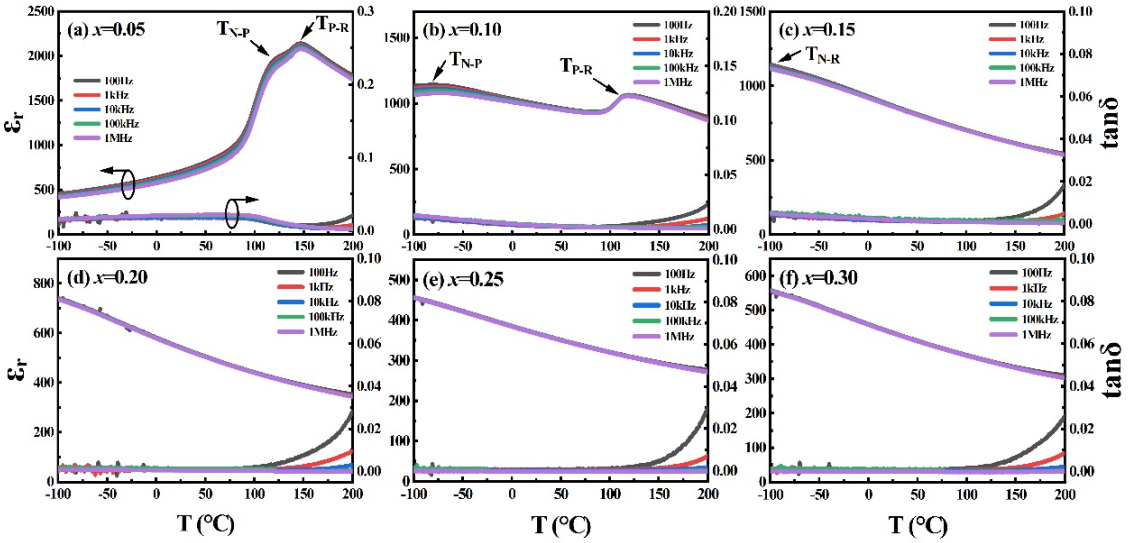

Fig. 3. Dielectric properties of the NNBT–*x*CLT ceramics tested in the range of −100–300°C.

146°C. Furthermore, another weaker dielectric abnormal peak with obvious frequency dispersion is observed and can be attributed to the phase transition from FE rhombohedral N-phase to AFE P-phase.[22,24] The phase transition temperature (T_{N-P}) is found to be in the vicinity of 122°C. It can be obviously seen in Figs. 3(b) and 3(c) that both T_{N-P} and T_{P-R} move to low values obviously accompanied by clear decrease in peak intensity and widening in peak width. These features endow the doped sample with much better thermal stability of the dielectric constant as compared to the undoped sample. The thermal stability indicated by $\Delta\varepsilon_r/\varepsilon_{r25°C}$ for the NNBT–xCLT ceramics at 1 kHz is plotted in Fig. S1. From the figure, one can note that the $x = 0.10$ ceramic exhibits an excellent thermal stability with $\Delta\varepsilon_r/\varepsilon_{r25°C} \leq \pm 15\%$ over a temperature range of −100–215°C meeting the EIA-X9R characterization standard (−55–200°C), indicating its promising potential for high-temperature applications.

For the CLT content $x \geq 0.15$, both phase transitions move to lower temperatures out of the tested temperature window. Meanwhile, the frequency dispersions of ε_r at T_{P-R} and T_{N-P} tend to be noticeable with increasing the CLT content. The diffuseness degree (γ) is calculated by the formula: $\frac{1}{\varepsilon_r} - \frac{1}{\varepsilon_m} = \frac{(T-T_m)^\gamma}{C}$, and found to be 1.43 and 1.48 for the samples of $x = 0.05$ and 0.10, respectively (Fig. S2). The broadened dielectric peaks and increased γ indicate an enhanced dielectric relaxation behavior. For $x \geq 0.15$, the T_{P-R} abnormal peak cannot be observed, indicating that the AFE R-phase is the sole phase above room temperature. In addition, the tanδ values of the NNBT–xCLT ceramics exhibit much low values than 0.03.

The P–E loops and the corresponding polarization current density–electric field (J–E) curves of the NNBT–xCLT ceramics are shown in Fig. 4. Due to the E_b value being lower than E_{AFE}, a well-saturated P–E loop with two sharp current density peaks can be observed in Fig. 4(a). For $x \geq 0.10$ ceramics, the P–E loop becomes thinner obviously featuring a linear-like polarization field response,[24] and the current density platform gradually replaces the sharp current density peak. The refinement of P–E loops indicates that the dielectric relaxation of the NNBT–xCLT ceramics is enhanced

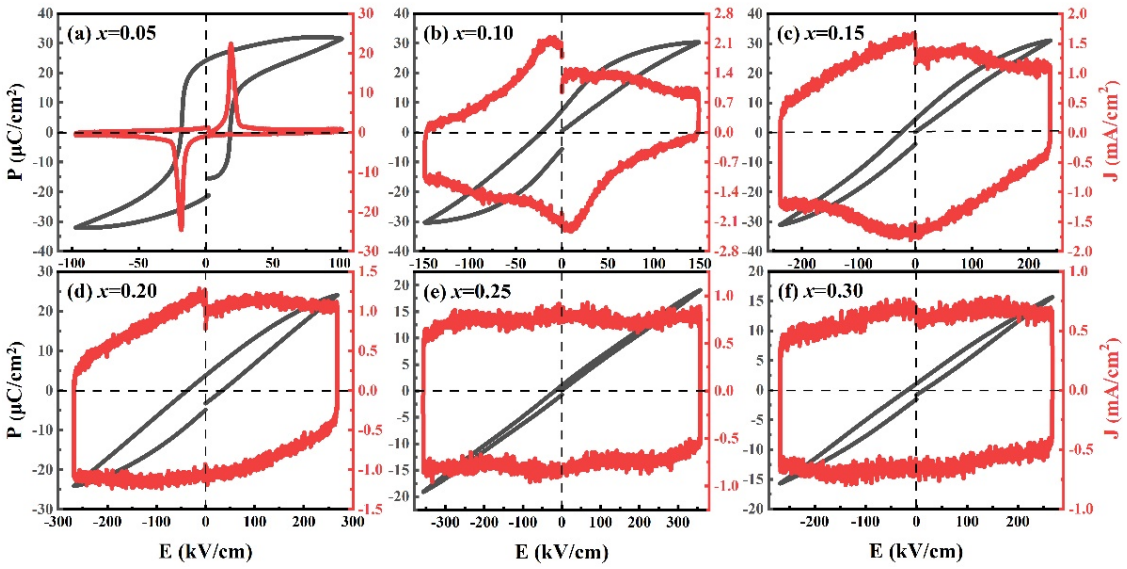

Fig. 4. P–E loops and the corresponding J–E curves of the NNBT–xCLT ceramics.

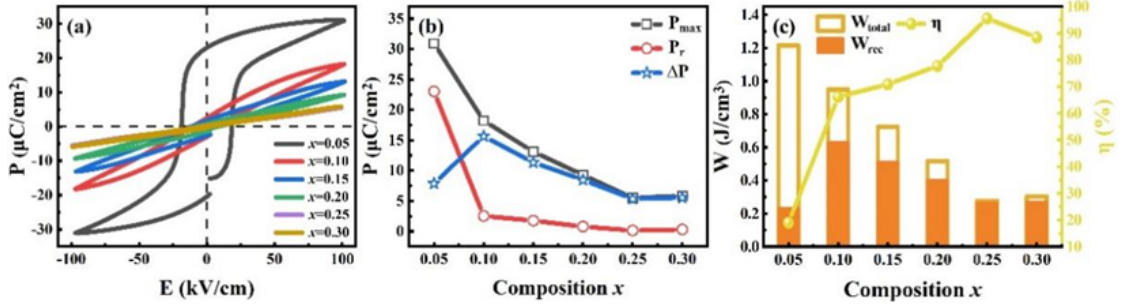

Fig. 5. (a) P–E loops at 100 kV/cm and 10 Hz of the NNBT–xCLT ceramics; (b) P_{max}, P_r, and ΔP; and (c) W_{total}, W_{rec}, and η values as a function of CLT content.

and the AFE R-phase is further stabilized. The stability of AFE R-phase and the enhancement of dielectric relaxation can significantly improve E_{AFE}, and both of them further expand the electric field response range of the NNBT–xCLT ceramics.[24] The bipolar P–E loops at 100 kV/cm and 10 Hz of the NNBT–xCLT ceramics are presented in Fig. 5(a). For $x \geq 0.10$, the P–E loops become thinner. Due to the close values of P_{max} and P_r for the samples of $x = 0.25$ and 0.30, their P–E loops seem to be overlapped with each other. An enlarged view of the P–E loops for the two samples is given in Fig. S3, from which the two P–E loops can be clearly seen.

The deduced P_{max}, P_r, and ΔP values of the NNBT–xCLT ceramics are shown in Fig. 5(b). The P_r value decreases with the increasing of CLT content, which may be related to the introduction of Ca^{2+}, La^{3+}, and Ti^{4+} into the $NaNbO_3$ matrix. The changes of valence and ionic radii for the NNBT–xCLT ceramics lead to nonuniform local composition and disordered charge, which disturb the long-range AFE order leading to randomly orientated polarization of the PNRs and improved relaxation behavior. Under an applied field, the polarizations of the PNRs rearrange their direction along the field giving rise to obvious P–E hysteresis, indicating that

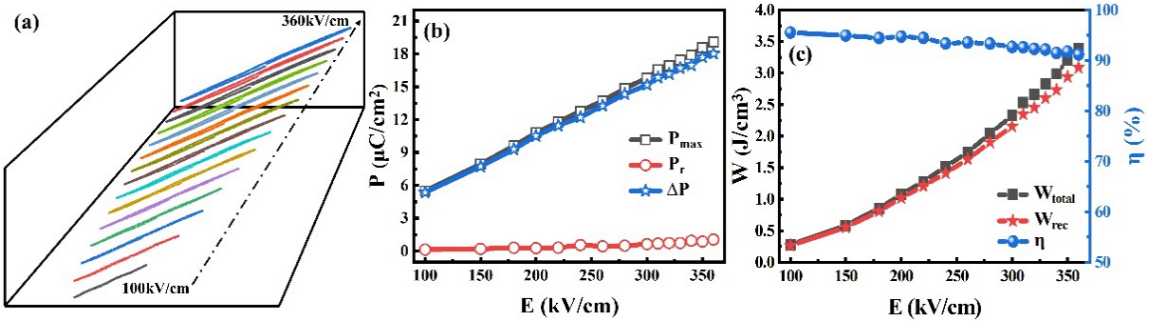

Fig. 6. Electric field-dependent (a) P–E loops, (b) P_{max}, P_r, and ΔP, and (c) W_{total}, W_{rec}, and η of the NNBT–0.25CLT sample.

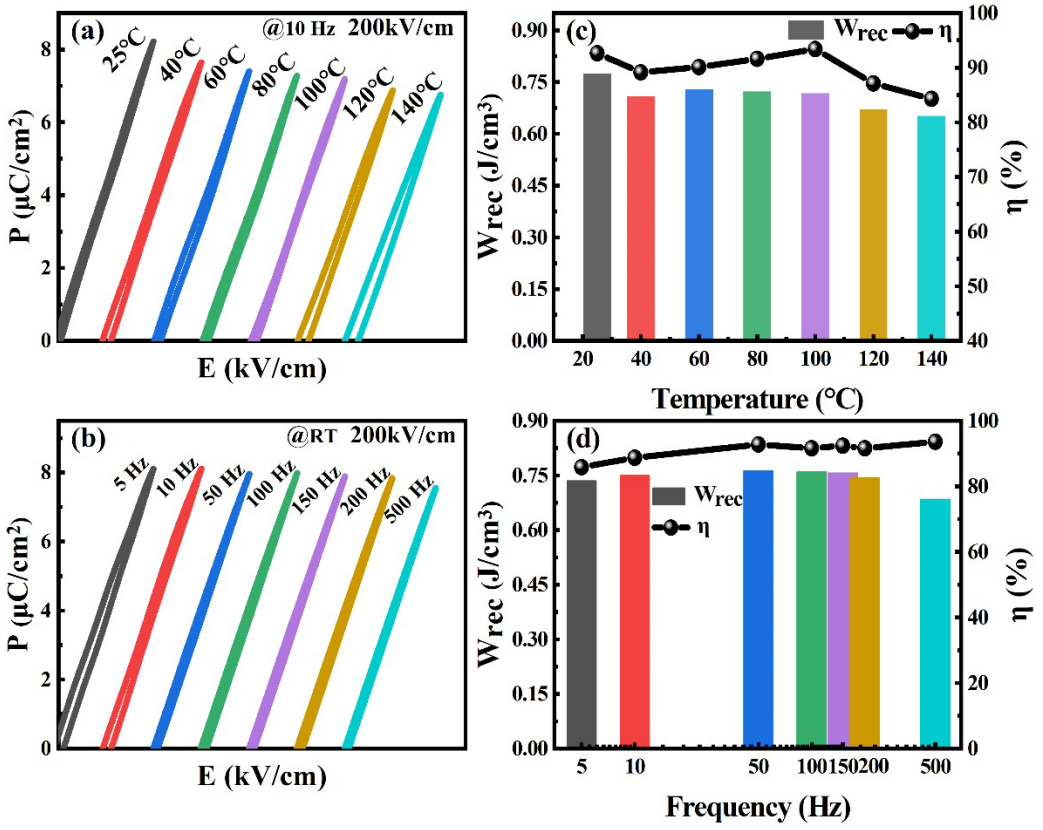

Fig. 7. P–E loops of the NNBT–0.25CLT ceramic measured under different (a) temperatures and (b) frequencies. The corresponding energy storage characteristics are also shown under different (c) temperatures and (d) frequencies.

the addition of CLT can effectively improve the comprehensive energy storage performance in the AFE R-phase stage. The calculated W_{rec} and η values as a function of the CLT content are plotted in Fig. 5(c). It is found that W_{rec} registers a peak at $x = 0.10$, while η reaches the maximum of 95.6% at $x = 0.25$. Considering the balance between W_{rec} and η, the composition of $x = 0.25$ ceramic is selected for further study.

In order to further study the energy storage performance of $x = 0.25$ sample, Fig. 6(a) shows the P–E loops under different electric fields up to E_b. Both P_{max} and ΔP increase linearly in the electric field range of 100–360 kV/cm, whereas P_r remains almost zero as shown in Fig. 6(b). This is because that the high electric field inhibits the long-range order of AFE nanodomains, and this means that $x = 0.25$ ceramic can quickly return to the original AFE state during the discharge of the electric field. Likewise, as seen in Fig. 6(c), the calculated W_{total} also increases approximately linearly; thus, the ceramic with $x = 0.25$ behaves as a linear dielectric. However, due to the AFE–FE phase transition, η value decreases slightly. And this also causes W_{rec} value to be gradually deviated from W_{total} value. Therefore, a huge $W_{rec} = 3.1$ J/cm^3 value and a superior $\eta = 91.5\%$ can be obtained simultaneously at 360 kV/cm, showing excellent potential for energy storage applications.

The temperature and frequency stability determines whether the ceramic capacitors can adapt to various environments. Figures 7(a) and 7(b) display the energy storage properties of the $x = 0.25$ ceramic at different temperatures and frequencies, respectively. The calculated W_{rec} and η values as a function of temperature are plotted in Figs. 7(c) and 7(d). From these figures, it is seen that W_{rec} of the sample decreases from 0.78 J/cm^3 to 0.65 J/cm^3 while η decreases from 92.7% to 84.3%, when the temperature increases from 25°C to 140°C. The variation of W_{rec} in the whole tested temperature range is 17.3%, but the η variation is no more than 10% in the whole tested temperature range. For frequency stability, W_{rec} of the sample changes from 0.74 J/cm^3 to 0.69 J/cm^3, while η increases from 85.9% to 93.6% in the range of 5–500 Hz. It can be seen from a careful observation that W_{rec} reaches its maximum at 50 Hz and then decreases, while η slightly increases with the increase of frequency. The above results show that the sample possesses good stability in the frequency range of 5–500 Hz and temperature range of 25–140°C, indicating the $x = 0.25$ ceramic is a good material for energy storage applications.

To further confirm the discharge rate and actual energy storage capacity of the sample, the discharge properties under the electric fields ranging from 100 kV/cm to 320 kV/cm are displayed in Fig. 8(a). The current density (C_D) and power density (P_D) can be calculated according to the relations: $C_D = I_{max}/S$ and $P_D = EI_{max}/2S$, where I_{max}, E, and S represent the first current peak amplitude, electric field strength, and electrode area of the sample, respectively. With E rising from

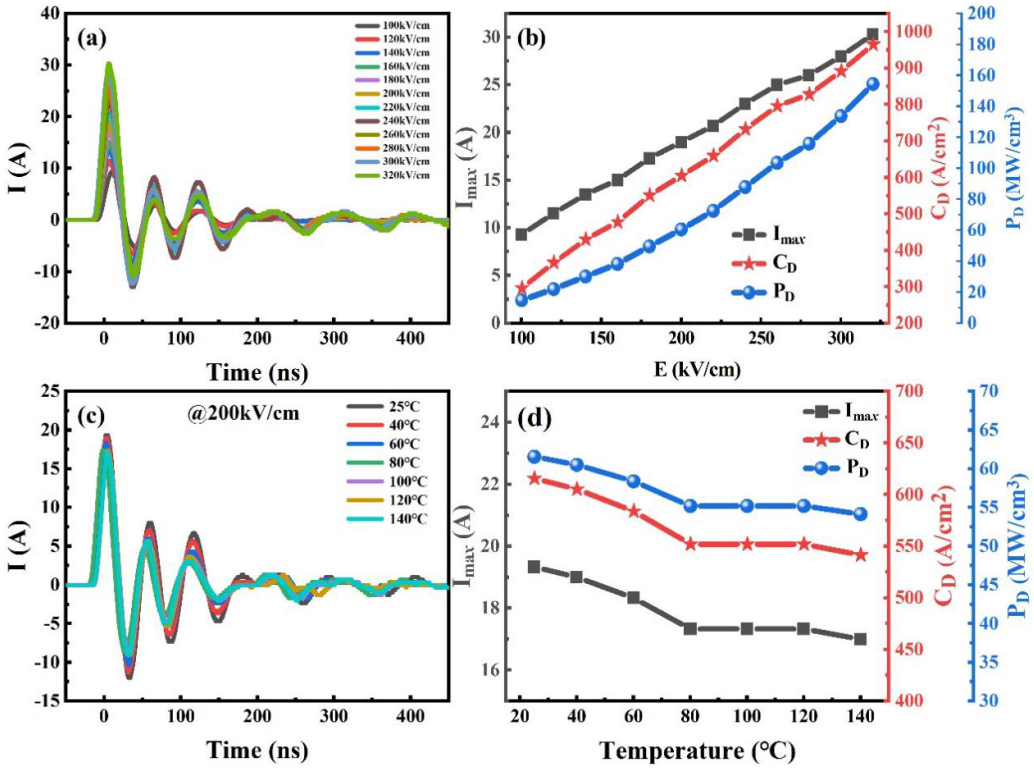

Fig. 8. (a) Room-temperature pulsed underdamped discharging current curves of the 0.25CLT ceramic under various electric fields; (b) the variations of I_{max}, C_D, and P_D with the applied electric field; and (c), (d) current curves of pulsed underdamped discharge of the NNBT–0.25CLT ceramic at different temperatures.

100 kV/cm to 320 kV/cm, the maximum values of I_{max}, C_D, and P_D of the $x = 0.25$ ceramic can reach 30.3 A, 965 A/cm^2, and 154 MW/cm^3, respectively [Fig. 8(b)]. For further research, the charge–discharge performance of the sample is tested in the temperature range of 25–140°C under 200 kV/cm [Fig. 8(c)]. The results are shown in Fig. 8(d). It shows that, when the measurement temperature is increased from 25°C to 140°C, P_D of the sample gradually decreases from 616 MW/cm^3 to 541 MW/cm^3, while the I_{max} and C_D values change in the same amplitude. These results illustrate that the $x = 0.25$ ceramic exhibits good temperature stability during the charging and discharging processes.

4. Conclusions

In summary, lead-free NNBT–*x*CLT energy storage ceramics were prepared by the conventional solid-state reaction method. The nonequivalent substitution of CLT at the *A*- and *B*-sites increases the disorder of the system. This, in turn, leads to slimmer *P–E* hysteresis loop and nearly linear polarization response. The $x = 0.25$ ceramic shows a high W_{rec} of 3.1 J/cm^3 and a high η of 91.5% with good thermal stability in the temperature range of 25–140°C and the frequency range of 5–500 Hz. A large C_D of 965 A/cm^2 and a large P_D of 154 MW/cm^3 were also achieved in the sample, giving the material tremendous promise for potential application in the field of pulsed power components.

Acknowledgments

This work was supported by the National Natural Science Foundation of China (NSFC) Grants 12174001 and 51872001 (C. Wang); and NSFC Grant 12104001 and Anhui Provincial Natural Science Foundation of Grant 2008085QE205 (F. Li).

Supporting Information

This material is available at https://www.worldscientific.com/doi/suppl/10.1142/S2010135X22420048

References

[1]X. Wang, X. Wang, Y. Huan, C. Li, J. Ouyang and T. Wei, A combined optimization strategy for improvement of comprehensive energy storage performance in sodium niobate-based antiferroelectric ceramics, *ACS Appl. Mater. Interfaces* **14**, 9330 (2022).

[2]H. Zhang, T. Wei, Q. Zhang, W. Ma, P. Fan, D. Salamon, S.-T. Zhang, B. Nan, H. Tan and Z.-G. Ye, A review on the development of lead-free ferroelectric energy-storage ceramics and multilayer capacitors, *J. Mater. Chem. C* **8**, 16648 (2020).

[3]G. Wang, Z. Lu, Y. Li, L. Li, H. Ji, A. Feteira, D. Zhou, D. Wang, S. Zhang and I. M. Reaney, Electroceramics for high-energy density capacitors: Current status and future perspectives, *Chem. Rev.* **121**, 6124 (2021).

[4]B. Chu, X. Zhou, K. Ren, B. Neese, M. Lin, Q. Wang, F. Bauer and Q. M. Zhang, A dielectric polymer with high electric energy density and fast discharge speed, *Science* **313**, 334 (2006).

[5]X. Hao, A review on the dielectric materials for high energy-storage application, *J. Adv. Dielectr.* **3**, 1330001 (2013).

[6]H. Tan, Z. Yan, S.-G. Chen, C. Samart, N. Takesue, D. Salamon, Y. Liu and H. Zhang, SPS prepared NN-24SBT lead-free relaxor-antiferroelectric ceramics with ultrahigh energy-storage density and efficiency, *Scr. Mater.* **210**, 114428 (2022).

[7]Q. Yuan, F. Z. Yao, S. D. Cheng, L. Wang, Y. Wang, S. B. Mi, Q. Wang, X. Wang and H. Wang, Bioinspired hierarchically structured all-inorganic nanocomposites with significantly improved capacitive performance, *Adv. Funct. Mater.* **30**, 2000191 (2020).

[8]P. Chen, W. Cao, T. Li, B. Zhao, J. Zheng and C. Wang, Outstanding energy-storage and charge–discharge performances in $Na_{0.5}Bi_{0.5}TiO_3$ lead-free ceramics via linear additive of $Ca_{0.85}Bi_{0.1}TiO_3$, *Chem. Eng. J.* **435**, 135065 (2022).

[9]W. Yang, H. Zeng, F. Yan, J. Lin, G. Ge, Y. Cao, W. Du, K. Zhao, G. Li, H. Xie and J. Zhai, Superior energy storage properties in $NaNbO_3$-based ceramics via synergistically optimizing domain and band structures, *J. Mater. Chem. A* **10**, 11613 (2022).

[10]W. Cao, T. Li, P. Chen and C. Wang, Outstanding energy storage performance of $Na_{0.5}Bi_{0.5}TiO_3$-$BaTiO_3$-$(Sr_{0.85}Bi_{0.1})(Mg_{1/3}Nb_{2/3})O_3$ lead-free ceramics, *ACS Appl. Energy Mater.* **4**, 9362 (2021).

[11]X. Yuan, Y. Zhang, L. Gong, B. Li and L. Zhang, High energy storage performance of $Na(Nb_{0.95}Ta_{0.05})O_3$/$Na_{0.5}Bi_{0.5}TiO_3$ lead-free ferroelectric ceramics, *Ceram. Int.* **48**, 13244 (2022).

[12]Y. Wan, F. Cao, J. Song, N. Hou, P. Ren, F. Yan, X. Lu, M. Ma, K. Song and G. Zhao, High-temperature dielectric properties of $Bi_{0.5}Na_{0.5}TiO_3$–$NaNbO_3$–$Sr_{0.8}Na_{0.4}Nb_2O_6$ ceramics, *Ceram. Int.* **48**, 13041 (2022).

[13]B. Chu, J. Hao, P. Li, Y. Li, W. Li, L. Zheng and H. Zeng, High-energy storage properties over a broad temperature range in La-modified BNT-based lead-free ceramics, *ACS Appl. Mater. Interfaces* **14**, 19683 (2022).

[14]F. Li, J. Zhai, B. Shen and H. Zeng, Recent progress of ecofriendly perovskite-type dielectric ceramics for energy storage applications, *J. Adv. Dielectr.* **08**, 1830005 (2019).

[15]X. Ji, F. Li, M. Long, C. Wang and L. Shan, Excellent temperature stability of energy storage performance by weak dipolar interaction strategy, *Appl. Phys. Lett.* **121**, 023902 (2022).

[16]W. Wang, L. Zhang, C. Li, D. O. Alikin, V. Y. Shur, X. Wei, F. Gao, H. Du and L. Jin, Effective strategy to improve energy storage properties in lead-free $(Ba_{0.8}Sr_{0.2})TiO_3$-$Bi(Mg_{0.5}Zr_{0.5})O_3$ relaxor ferroelectric ceramics, *Chem. Eng. J.* **446**, 137389 (2022).

[17]H. Dong, B. Luo and K. Jin, Structural, electrical and energy storage properties of lead-free $NaNbO_3$-$BaHfO_3$ thin films, *J. Phys. Chem. Solids* **162**, 110513 (2022).

[18]D. Lai, Z. Yao, W. You, B. Gao, Q. Guo, P. Lu, A. Ullah, H. Hao, M. Cao and H. Liu, Regulating energy storage performances of $0.85NaNbO_3$-$0.15Bi(Zn_{2/3}Nb_{1/3})O_3$ ceramics using $BaTiO_3$, *J. Materiomics* **8**, 166 (2022).

[19]L. Wang, H. Qi, B. Gao, Y. Liu, H. Liu and J. Chen, Large piezoelectricity in $NaNbO_3$-based lead-free ceramics via tuning oxygen octahedral tilt, *Mater. Horiz.* **9**, 1002 (2022).

[20]A. Manan, M. U. Rehman, A. Ullah, A. S. Ahmad, Y. Iqbal, I. Qazi, M. A. Khan, H. U. Shah and A. H. Wazir, High energy storage density with ultra-high efficiency and fast charging–discharging capability of sodium bismuth niobate lead-free ceramics, *J. Adv. Dielectr.* **11**, 2150018 (2021).

[21]N. Luo, K. Han, M. J. Cabral, X. Liao, S. Zhang, C. Liao, G. Zhang, X. Chen, Q. Feng, J. F. Li and Y. Wei, Constructing phase boundary in $AgNbO_3$ antiferroelectrics: Pathway simultaneously achieving high energy density and efficiency, *Nat. Commun.* **11**, 4824 (2020).

[22]H. Qi, A. Xie, J. Fu and R. Zuo, Emerging antiferroelectric phases with fascinating dielectric, polarization and strain response in $NaNbO_3$-$(Bi_{0.5}Na_{0.5})TiO_3$ lead-free binary system, *Acta Mater.* **208**, 116710 (2021).

[23]H. Ding, M. H. Zhang, J. Koruza, L. Molina-Luna and H. J. Kleebe, Domain morphology of newly designed lead-free antiferroelectric $NaNbO_3$-$SrSnO_3$ ceramics, *J. Am. Ceram. Soc.* **104**, 3715 (2021).

[24]A. Xie, J. Fu, R. Zuo, C. Zhou, Z. Qiao, T. Li and S. Zhang, $NaNbO_3$-$CaTiO_3$ lead-free relaxor antiferroelectric ceramics featuring giant energy density, high energy efficiency and power density, *Chem. Eng. J.* **429**, 132534 (2022).

[25]J. Jiang, X. Li, L. Li, S. Guo, J. Zhang, J. Wang, H. Zhu, Y. Wang and S.-T. Zhang, Novel lead-free $NaNbO_3$-based relaxor antiferroelectric ceramics with ultrahigh energy storage density and high efficiency, *J. Materiomics* **8**, 295 (2022).

[26]Y. Fan, Z. Zhou, R. Liang and X. Dong, Designing novel lead-free $NaNbO_3$-based ceramic with superior comprehensive energy storage and discharge properties for dielectric capacitor applications via relaxor strategy, *J. Eur. Ceram. Soc.* **39**, 4770 (2019).

[27]X. Dong, X. Li, X. Chen, H. Chen, C. Sun, J. Shi, F. Pang and H. Zhou, High energy storage and ultrafast discharge in $NaNbO_3$-based lead-free dielectric capacitors via a relaxor strategy, *Ceram. Int.* **47**, 3079 (2021).

[28]W. Li, X. Xia, J. Zeng, L. Zheng, Z. Man and G. Li, 1/6 type diffraction patterns and double P-E hysteresis loops in $Bi(Mg_{2/3}Nb_{1/3})O_3$ modified $NaNbO_3$ ceramics, *J. Phys. D, Appl. Phys.* **53**, 305302 (2020).

[29]S. Li, P. Shi, X. Zhu, B. Yang, X. Zhang, R. Kang, Q. Liu, Y. Gao, H. Sun and X. Lou, Enhanced energy storage properties in lead-free $NaNbO_3$–$Sr_{0.7}Bi_{0.2}TiO_3$–$BaSnO_3$ ternary ceramic, *J. Mater. Sci.* **56**, 11922 (2021).

[30]S. K. Mishra, N. Choudhury, S. L. Chaplot, P. S. R. Krishna and R. Mittal, Competing antiferroelectric and ferroelectric interactions in $NaNbO_3$: Neutron diffraction and theoretical studies, *Phys. Rev. B* **76**, 024110 (2007).

[31]H. Chen, X. Wang, X. Dong, Y. Pan, J. Wang, L. Deng, Q. Dong, H. Zhang, H. Zhou and X. Chen, Adjusting the energy-storage characteristics of $0.95NaNbO_3$-$0.05Bi(Mg_{0.5}Sn_{0.5})O_3$ ceramics by doping linear perovskite materials, *ACS Appl. Mater. Interfaces* **14**, 25609 (2022).

[32]J. Jiang, X. Meng, L. Li, J. Zhang, S. Guo, J. Wang, X. Hao, H. Zhu and S.-T. Zhang, Enhanced energy storage properties of lead-free $NaNbO_3$-based ceramics via A/B-site substitution, *Chem. Eng. J.* **422**, 130130 (2021).

[33]S. Xie, K. Zhu, J. Qiu and H. Guo, Microstructure and electrical properties of $NaNbO_3$-$BaTiO_3$ lead-free piezoelectric ceramics, *Front. Mech. Eng. China* **4**, 345 (2009).

[34]J. T. Zeng, K. W. Kwok and H. L. W. Chan, Ferroelectric and piezoelectric properties of $Na_{1-x}Ba_xNb_{1-x}Ti_xO_3$ ceramics, *J. Am. Ceram. Soc.* **89**, 2828 (2006).

[35]B. Luo, X. Wang, E. Tian, H. Song, H. Wang and L. Li, Enhanced energy-storage density and high efficiency of lead-Free $CaTiO_3$-$BiScO_3$ linear dielectric ceramics, *ACS Appl. Mater. Interfaces* **9**, 19963 (2017).

[36]J. Zhang, J. Wang, D. Gao, H. Liu, J. Xie and W. Hu, Enhanced energy storage performances of $CaTiO_3$-based ceramic through A-site Sm^{3+} doping and A-site vacancy, *J. Eur. Ceram. Soc.* **41**, 352 (2021).

[37]S. Tripathi, D. Pandey, S. K. Mishra and P. S. R. Krishna, Morphotropic phase-boundary-like characteristic in a lead-free and non-ferroelectric $(1-x)NaNbO_3$–$xCaTiO_3$ system, *Phys. Rev. B* **77**, 052104 (2008).

[38]D. Sri Gyan, A. A. Goyal, Y. Tamrakar and A. Dwivedi, Stabilization of anti-ferroelectric *Pbcm* phase over ferroelectric $P2_1ma$ phase in intermittent ferroelectric $NaNbO_3$ by incorporating $CaTiO_3$, *J. Phys. D, Appl. Phys.* **52**, 165304 (2019).

[39]H. Chen, X. Dong, X. Wang, Y. Pan, J. Wang, L. Deng, X. Chen, Q. Dong, H. Zhang and H. Zhou, Energy storage properties in $Bi(Mg_{1/2}Sb_{2/3})O_3$-doped $NaNbO_3$ lead-free ceramics, *Ceram. Int.* **48**, 7723 (2022).

[40]M. Zhou, R. Liang, Z. Zhou and X. Dong, Developing a novel high performance $NaNbO_3$-based lead-free dielectric capacitor for energy storage applications, *Sustain. Energy Fuels* **4**, 1225 (2020).

[41]M. Zhou, R. Liang, Z. Zhou, S. Yan and X. Dong, Novel sodium niobate-based lead-free ceramics as new environment-friendly energy storage materials with high energy density, high power density, and excellent stability, *ACS Sustain. Chem. Eng.* **6**, 12755 (2018).

[42]L. Yang, X. Kong, F. Li, H. Hao, Z. Cheng, H. Liu, J.-F. Li and S. Zhang, Perovskite lead-free dielectrics for energy storage applications, *Prog. Mater. Sci.* **102**, 72 (2019).